

Pre-training Graph Neural Networks on 2D and 3D Molecular Structures by using Multi-View Conditional Information Bottleneck

Van Thuy Hoang and O-Joun Lee*

Department of Artificial Intelligence, The Catholic University of Korea
{hoangvanthuy90, ojlee}@catholic.ac.kr

Abstract

Recent pre-training strategies for molecular graphs have attempted to use 2D and 3D molecular views as both inputs and self-supervised signals, primarily aligning graph-level representations. However, existing studies remain limited in addressing two main challenges of multi-view molecular learning: (1) discovering shared information between two views while diminishing view-specific information and (2) identifying and aligning important substructures, e.g., functional groups, which are crucial for enhancing cross-view consistency and model expressiveness. To solve these challenges, we propose a Multi-View Conditional Information Bottleneck framework, called MVCIB, for pre-training graph neural networks on 2D and 3D molecular structures in a self-supervised setting. Our idea is to discover the shared information while minimizing irrelevant features from each view under the MVCIB principle, which uses one view as a contextual condition to guide the representation learning of its counterpart. To enhance semantic and structural consistency across views, we utilize key substructures, e.g., functional groups and ego-networks, as anchors between the two views. Then, we propose a cross-attention mechanism that captures fine-grained correlations between the substructures to achieve subgraph alignment across views. Extensive experiments in four molecular domains demonstrated that MVCIB consistently outperforms baselines in both predictive performance and interpretability. Moreover, MVCIB achieved the 3d Weisfeiler-Lehman expressiveness power to distinguish not only non-isomorphic graphs but also different 3D geometries that share identical 2D connectivity, such as isomers.

Introduction

Pre-training Graph Neural Networks (GNNs) for molecules has emerged as a promising approach to address the challenge of limited labels of molecular data (Rong et al. 2020; Luong and Singh 2023). Most recent methods have mainly focused on 2D molecular graphs, which represent atoms as nodes and chemical bonds as edges. However, relying only on 2D information can be insufficient to determine chemical properties of molecules (Liu et al. 2022). As shown in Fig. 1 (a), cis and trans isomers have the same 2D connectivity, yet differ in the 3D atom positions, leading to different properties. That is, cis isomers tend to be more soluble in polar

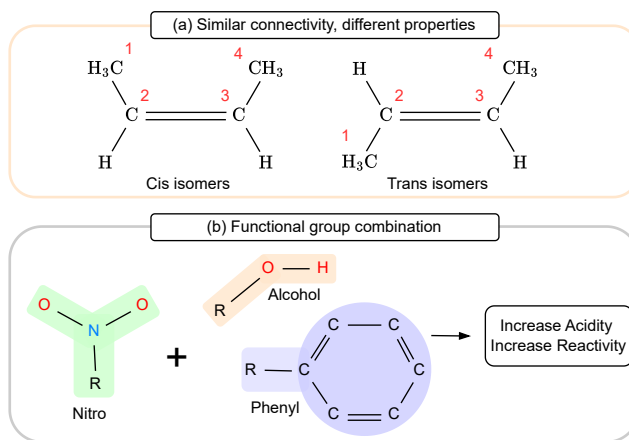


Figure 1: (a) It is difficult to distinguish cis and trans isomers only based on the 2D molecular graphs. (b) The incorporation of a Nitro group ($R-NO_2$) into an Aromatic Hydroxyl group ($R-C_6H_5$, $R-OH$) could change its chemical property.

solvents and exhibit a higher boiling point than trans isomers. However, representations of 2D molecular structures are difficult to reflect such 3D geometric features.

Recently, 2D and 3D molecular information have been jointly used in the pre-training of GNNs to enhance the quality of representations (Kim et al. 2024; Stärk et al. 2022). Most strategies aim to leverage the complementary information between the two views by employing contrastive learning objectives to maximize agreement between graph-level representations (Stärk et al. 2022; Liu et al. 2022). For example, GraphMVP (Liu et al. 2022) introduces a joint training framework that combines contrastive learning with a reconstruction objective to align graph-level representations. More recently, a few methods have extended contrastive objectives to the subgraph level, aiming to align semantic substructures, e.g., functional groups, to learn chemically informed representations (Kim et al. 2024; Luong and Singh 2023). To sum up, most recent studies adopt the contrastive objectives to maximize the agreement between views on graph- or subgraph-level representations.

However, two main challenges limit the recent studies. (1) Most recent multi-view strategies are limited to extracting

*Corresponding author: O-Joun Lee (Tel.: +82-2-2164-5516)

shared and task-relevant information while minimizing irrelevant features from each view. From the multi-view learning perspective, each view is expected to contain a mixture of shared information and view-specific information, as they originate from the same molecule and share the same label (Tsai et al. 2021). Recent studies show that maximizing the shared features is crucial for enhancing the model generalization for downstream tasks (Federici et al. 2020). However, recent studies focus only on maximizing mutual information between representations from different views, without considering shared and view-specific information. (2) The recent studies are limited in their ability to identify and align important substructures across views. That is, while graph structures can differ between 2D and 3D views, the important substructures, e.g., functional groups, are invariant and commonly play a critical role in determining molecular properties (Kim et al. 2024). Through empirical experiments, we showed that capturing and aligning these substructures could enhance the model’s expressiveness in distinguishing not only non-isomorphic graphs but also isomers with identical 2D connectivity but differ in 3D geometry (Appendix D.6). Moreover, the co-occurrences of functional groups can be significant features for property prediction. For example, Fig. 1 (b) shows that adding a nitro group (NO_2) to a molecule containing a phenyl (C_6H_5) and alcohol (OH) can alter the chemical properties.

In this paper, we propose the Multi-View Conditional Information Bottleneck (MVCIB), a GNN pre-training method designed to maximize shared information and align important substructures across molecular views. MVCIB is characterized by two main contributions. (1) The key contribution of MVCIB lies in its ability to maximize the shared and task-relevant information while minimizing irrelevant information from specific views in a self-supervised setting. We address this problem with the Information Bottleneck (IB) principle for learning compressed yet informative representations. However, applying the IB principle in a self-supervised setting is challenging due to the absence of labels, making it difficult to capture task-relevant information. To solve it, we propose the MVCIB principle, which utilizes a conditional compression strategy by using one molecular view as a conditional context to guide the representation learning of the other view. This is based on the multi-view assumption that, although each view could differ in perspective, all views originate from the same underlying molecule.

To align important substructures across views, we first sample key subgraphs from molecular views to serve as anchor points, followed by a cross-attention mechanism to align the representations across views. (2-1) We extract two types of important subgraphs, i.e., functional groups and ego-networks rooted at each node, to enable MVCIB to capture both chemical semantics and contextual structures, enhancing the model’s transferability and expressiveness, respectively. That is, the model could benefit from learning correct patterns, e.g., functional groups, during the pre-training phase, enhancing its ability to transfer knowledge from large-scale unlabeled datasets to downstream datasets. To extract functional groups, we employ the BRICS algorithm (Degen et al. 2008) to decompose molecules into

chemical subgraphs. (2-2) We propose a cross-attention mechanism to align subgraph-level representations across views, where each subgraph representation from one view is used to attend over representations in the other view. By doing so, the cross-attention scores could enable MVCIB to learn fine-grained cross-view correlations between subgraph representations and align the important substructures.

Related work

Recent studies have jointly used 2D and 3D molecular information to pre-train GNNs for improving molecular property prediction (Liu et al. 2022; Zhu et al. 2022). The main idea is to learn representations from two views and then align the graph-level representations under the contrastive objectives (Xia et al. 2023; Stärk et al. 2022). For example, GraphMVP (Liu et al. 2022) employs a joint contrastive learning and reconstruction task to align graph-level representations from two views. The idea of 3D Infomax (Stärk et al. 2022) is to infer the molecular geometry from 2D molecular graphs by maximizing the agreement between two view representations. However, most recent strategies overlook discovering shared information and do not identify functional groups, which are crucial for determining property prediction. Besides, several augmentation-based strategies extend 2D molecular learning to a multi-view problem by using augmentation schemes, e.g., edge perturbation, with contrastive objectives (Liu et al. 2022; Qiu et al. 2020). However, these studies do not learn the complementary information from 2D and 3D molecular structures, limiting their ability to capture the 3D geometric features. In contrast, MVCIB is designed to preserve and align chemical substructures between views, followed by maximizing the shared information and minimizing irrelevant features across views.

Recently, important molecular substructures, e.g., functional groups, have been incorporated into pre-training methods to improve knowledge transfer to downstream tasks (Zhang et al. 2021; Liu et al. 2023). These substructures are commonly determined by using chemical rules or manual annotation (Inae, Liu, and Jiang 2023). For example, GraphFP (Luong and Singh 2023) decomposes 2D molecular structures into a bag of fragments based on a subgraph dictionary, constructed from frequently occurring substructures across molecular datasets. However, these strategies primarily focus on 2D molecular structures and are thus limited in capturing the 3D geometric features. More recently, several studies (Kim et al. 2024; Huang et al. 2024) have proposed using both 2D and 3D molecular views to effectively encode the chemical substructures into representations. For instance, HoliMol (Kim et al. 2024) extracts important substructures from both views by decomposing molecules into fragments and then aligns the graph-level representations using a contrastive objective. However, these methods rely only on contrasting graph-level representations without considering the shared information between two views, which could retrain noisy information and degrade generalization performance across downstream tasks (Federici et al. 2020). In contrast, MVCIB not only focuses on subgraph-level alignment but also maximizes the shared

information between molecular views and minimizes the irrelevant information.

Problem Descriptions

We study the problem of multi-view molecular learning under the MVCIB principle. Thus, we first introduce the notation, followed by a definition of MVCIB, which extends the IB principle to the multi-view setting.

Let $G_{2D} = (X, E_{2D})$ denote a 2D molecular graph with initial atom features X and the set of edges E_{2D} . Let $G_{3D} = (X, E_{3D}, R)$ denote the corresponding 3D molecular graph, where E_{3D} denotes the set of edges, and $R \in \mathbb{R}^{N \times 3}$ contains the 3D coordinates of the N atoms.

Recently, the Information Bottleneck (IB) principle (Tishby, Pereira, and Bialek 2000) has been applied to graphs to learn compressed yet informative representations.

Definition 1 (IB). *Given an input graph G and its label Y , the IB principle learns the compressed yet sufficient representation \mathbf{Z} by optimizing the following objective:*

$$\min_{\mathbf{Z}} I(G, \mathbf{Z}) - \beta I(\mathbf{Z}, Y), \quad (1)$$

where the first term encourages compression of the input, the second term is for predictive sufficiency, and β is a hyperparameter controlling the balance between the two terms.

In the context of self-supervised learning, our goal is to optimize the first term in Eq. 1, omitting the use of label Y . From a multi-view perspective, let G_{2D} and G_{3D} denote the 2D and 3D views from the same molecule, respectively. Each view can contain view-specific information, which can be considered as noise from its counterpart view. However, as both views originate from the same molecule and share identical labels, their representations need to encode the shared features that are most relevant for downstream tasks. Here, we present the formulation for the 2D view only, as the formulation for the 3D view follows analogously. From the 2D view, we aim to compress G_{2D} into a compressed yet shared representation \mathbf{Z}_{2D}^{CIB} conditioned by the G_{3D} .

Definition 2 (MVCIB). *When G_{3D} is already observed, the mutual information $I(G_{2D} | \mathbf{Z}_{2D}^{CIB})$ can be factorized to reveal shared information in the 2D view. By conditioning on G_{3D} , the shared information can be discovered as:*

$$\mathbf{Z}_{2D}^{CIB} = \arg \min_{\mathbf{Z}_{2D}^{CIB}} \underbrace{I(G_{2D}; \mathbf{Z}_{2D}^{CIB} | G_{3D})}_{\text{Conditional compression}} - \beta \underbrace{I(\mathbf{Z}_{2D}^{CIB}; G_{3D})}_{\text{Sufficient prediction}}. \quad (2)$$

The second term, $I(\mathbf{Z}_{2D}^{CIB}; G_{3D})$, aims to maximize sufficiency, ensuring that the representation \mathbf{Z}_{2D}^{CIB} retains as much shared information as possible from the complementary view G_{3D} , thereby increasing its sufficiency for label prediction. Thus, the mutual information $I(G_{2D} | \mathbf{Z}_{2D}^{CIB})$ can be reduced by minimizing the first term $I(G_{2D}; \mathbf{Z}_{2D}^{CIB} | G_{3D})$. This penalizes the information in \mathbf{Z}_{2D}^{CIB} that is unique to G_{2D} and not relevant to the G_{3D} . Similarly, from 3D view, we can exploit a shared information \mathbf{Z}_{3D}^{CIB} when G_{2D} is already observed.

Methodology

Multi-View Subgraph Sampling

Fig. 2 presents the architecture of MVCIB. For subgraph sampling, we simultaneously sample the two types of subgraphs, i.e., contextual and semantic subgraphs, for each node within both the 2D and 3D molecular graphs. To sample contextual subgraphs in the 2D graphs, for each given node v , we extract k -hop ego-network $G_{2D}[N_k(v)]$ rooted at v , where $N_k(v)$ denotes the set of neighbor nodes within k -hop distance. In contrast, for the 3D graphs, we sample contextual subgraphs $G_{3D}[N_r(v)]$ containing atoms that lie within an r -Å radius of node v .

To extract semantic subgraphs, i.e., functional groups, we employ the BRICS algorithm (Degen et al. 2008), which incorporates domain knowledge to decompose molecules into chemical substructures. Formally, given a 2D molecular graph G_{2D} , we define the set of functional group fragments as $F = \{G^{(0)}, G^{(1)}, \dots, G^{(m)}\}$, where $G^{(i)} = (V^{(i)}, E^{(i)})$ denotes the i -th subgraph, m is the number of fragments, and $V^{(i)} \cap V^{(j)} = \{\emptyset\}$. For the 3D graph, we extract the same functional groups as the 2D graph, as they are structurally invariant and can be consistently recognized across views.

Multi-View Subgraph Alignment

Subgraph Learning For 2D molecular graphs, we adopt the GIN encoder (Xu et al. 2019), which is a powerful GNN model with high structure distinguishability. Specifically, given a target node v in G_{2D} , we obtain two types of representations, i.e., contextual and semantic representations. To learn the contextual representation of a node v , we first learn the representation of any node u within the ego-network $G_{2D}[N_k(v)]$ rooted at v . Then, the contextual representation of node v is obtained via a readout function, as:

$$\mathbf{H}_{2D}^u = \text{GNN}(G_{2D}[N_k(v)] | u \in N_k(v)), \quad (3)$$

$$\mathbf{H}_{2D}^{v|\text{Context}} = \text{Readout}(\mathbf{H}_{2D}^u | u \in N_k(v)), \quad (4)$$

where $\text{GNN}(\cdot)$ is the GIN encoder and $\text{Readout}(\cdot)$ is a summation function. Similarly, to obtain the semantic representations of node v , we apply the GIN encoder on its functional group subgraph $G^{(i)}$, as follows:

$$\mathbf{H}_{2D}^u = \text{GNN}(G^{(i)} | u \in G^{(i)}), \quad (5)$$

$$\mathbf{H}_{2D}^{v|\text{Semantics}} = \text{Readout}(\mathbf{H}_{2D}^u | u \in G^{(i)}). \quad (6)$$

By doing so, our encoder can capture the contextual and semantic subgraph-level information rooted at each node v . We then incorporate the representations of the node v , as:

$$\mathbf{H}_{2D}^v = \text{FUSE}(\mathbf{H}_{2D}^{v|\text{Context}}, \mathbf{H}_{2D}^{v|\text{Semantics}}), \quad (7)$$

where $\text{FUSE}(\cdot)$ is concatenation.

For the 3D molecular graph, we employ an Equivariant Graph Neural Network (EGNN) encoder (Satorras, Hoogeboom, and Welling 2021), a powerful architecture designed to preserve equivariance to geometric transformations, e.g., rotations. Analogously, for the node v , we apply EGNN to obtain the contextual representation $\mathbf{H}_{3D}^{v|\text{Context}}$

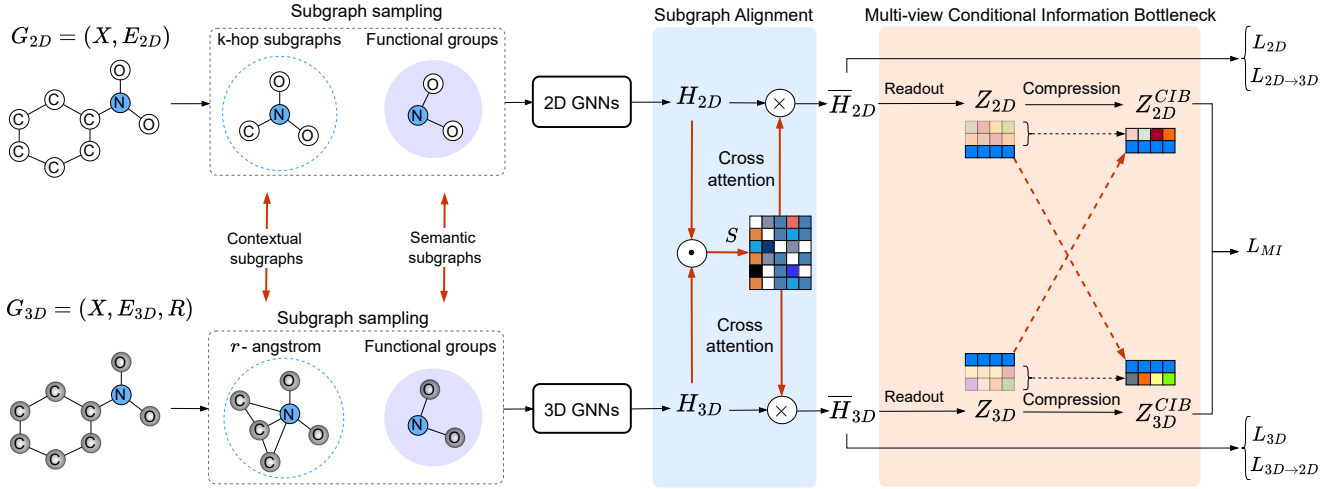


Figure 2: An overall architecture of MVCIB, consisting of (i & ii) subgraph sampling and alignment and (iii) MVCIB principle.

in $G_{3D}[N_r(v)]$ and semantic representation $\mathbf{H}_{3D}^v|_{\text{Semantics}}$ in $G_{3D}^{(i)}$. Then, the subgraph-level representation of a node v from the 3D view can be defined as:

$$\mathbf{H}_{3D}^v = \text{FUSE} \left(\mathbf{H}_{3D}^v|_{\text{Context}}, \mathbf{H}_{3D}^v|_{\text{Semantics}} \right). \quad (8)$$

Subgraph Alignment We now align important substructures by using a cross-attention mechanism, where each atom representation in one view is used to attend over representations in the other view. Specifically, we compute an affinity matrix \mathbf{S} to quantify how similar the representations of each atom are across the different views, as:

$$\mathbf{S} = (W_{2D}\mathbf{H}_{2D})(W_{3D}\mathbf{H}_{3D})^\top, \quad (9)$$

where W_{2D} and W_{3D} are learnable matrices and \mathbf{S}_{ij} denotes the similarity of the i -th atom from \mathbf{H}_{2D} and the j -th atom from \mathbf{H}_{3D} . For 2D-queried cross-attention, we employ a cross-attention mechanism, where each 2D representation serves as a query to compute attention weights over the 3D representations. Then, we construct an attended 3D representation $\bar{\mathbf{H}}_{3D}^i$ based on given 2D representation \mathbf{H}_{2D}^i by applying a weighted combination over 3D representations:

$$\bar{\mathbf{H}}_{3D}^i = \sum_{j=1}^N \xi_{ij} \mathbf{H}_{3D}^j, \quad \xi_{ij} = \frac{\exp(\mathbf{S}_{ij})}{\sum_{j=1}^N \exp(\mathbf{S}_{ij})}. \quad (10)$$

Likewise, we can compute the 2D representations that are attended by 3D representations by considering each 3D representation as a query:

$$\bar{\mathbf{H}}_{2D}^j = \sum_{i=1}^N \zeta_{ij} \mathbf{H}_{2D}^i, \quad \zeta_{ij} = \frac{\exp(\mathbf{S}_{ij})}{\sum_{i=1}^N \exp(\mathbf{S}_{ij})}. \quad (11)$$

Multi-View Conditional Information Bottleneck

We now present our MVCIB principle by maximizing the shared information across views in an SSL setting. Specifically, from the 2D view, we compress G_{2D} into shared information \mathbf{Z}_{2D}^{CIB} and discard the noise from G_{2D} that is not

relevant to the 3D view. Based on Definition 2, we can minimize $I(G_{2D}|\mathbf{Z}_{2D}^{CIB})$ under MVCIB principle, as:

$$I(G_{2D}|\mathbf{Z}_{2D}^{CIB}) = I(G_{2D}; \mathbf{Z}_{2D}^{CIB}|G_{3D}) - \beta_1 I(\mathbf{Z}_{2D}^{CIB}; G_{3D}). \quad (12)$$

Similarly, from the 3D view, we can minimize the mutual information $I(G_{3D}|\mathbf{Z}_{3D}^{CIB})$ as:

$$I(G_{3D}|\mathbf{Z}_{3D}^{CIB}) = I(G_{3D}; \mathbf{Z}_{3D}^{CIB}|G_{2D}) - \beta_2 I(\mathbf{Z}_{3D}^{CIB}; G_{2D}). \quad (13)$$

We now jointly minimize Eq. 12 and Eq. 13. By combining and modifying the Lagrangian multipliers β_1 and β_2 , we propose to minimize the loss function L_{MI} , as:

$$L_{MI} = [I(G_{2D}; \mathbf{Z}_{2D}^{CIB}|G_{3D}) + I(G_{3D}; \mathbf{Z}_{3D}^{CIB}|G_{2D})] - \alpha [I(\mathbf{Z}_{2D}^{CIB}; G_{3D}) + I(\mathbf{Z}_{3D}^{CIB}; G_{2D})], \quad (14)$$

where α controls the trade-off between the two terms. By considering \mathbf{Z}_{2D}^{CIB} and \mathbf{Z}_{3D}^{CIB} into a shared latent space, we can derive an upper bound on L_{MI} , as:

$$L_{MI} \leq D_{SKL}(p(\mathbf{Z}_{2D}^{CIB}|G_{2D}) \| p(\mathbf{Z}_{3D}^{CIB}|G_{3D})) - \alpha I(\mathbf{Z}_{2D}^{CIB}; \mathbf{Z}_{3D}^{CIB}), \quad (15)$$

where $D_{SKL}(\cdot \| \cdot)$ denotes a symmetrized KL divergence between two distributions. The proof of Eq. 15 is provided in Appendix A.1. For the first term, we can directly compute the average of the expected KL divergences between distributions $D_{KL}(p(\mathbf{Z}_{2D}^{CIB}|\mathbf{Z}_{2D}) \| p(\mathbf{Z}_{3D}^{CIB}|\mathbf{Z}_{3D}))$ and $D_{KL}(p(\mathbf{Z}_{3D}^{CIB}|\mathbf{Z}_{3D}) \| p(\mathbf{Z}_{2D}^{CIB}|\mathbf{Z}_{2D}))$, that both distributions have known densities. To optimize the second term, i.e., $-I(\mathbf{Z}_{2D}^{CIB}; \mathbf{Z}_{3D}^{CIB})$, we adopt the Jensen–Shannon estimator (Hjelm et al. 2019), which can enable a tractable approximation of mutual information via neural networks.

The final representation is obtained by concatenating \mathbf{Z}_{2D}^{CIB} and \mathbf{Z}_{3D}^{CIB} , which is then used for downstream tasks.

Multi-Task Objectives

2D-View SSL From the 2D view, we employ a graph reconstruction loss L_{2D} to encourage MVCIB to preserve the

2D graph structure. Specifically, given the representation matrix \bar{H}_{2D} , we compute the pairwise similarity between any two nodes v_i and v_j by using cosine similarity, i.e.,

$$P_{i,j} = \frac{\bar{H}_{2D}^i \bar{H}_{2D}^j}{\|\bar{H}_{2D}^i\| \|\bar{H}_{2D}^j\|}, \quad (\text{Zhang et al. 2020}).$$

Then, the reconstruction loss can be defined as follows:

$$L_{2D} = \frac{1}{|V|^2} \|A - P\|_F^2, \quad (16)$$

where A denotes the original adjacency matrix of G_{2D} .

3D-View SSL We adopt a 3D position denoising as a SSL task for 3D graph recovery, following Godwin et al. (2022); Zaidi et al. (2023). Specifically, Gaussian noise is added to the input positions of atoms, and the model is trained to predict the noise from the perturbed input. Let $\mathbf{R} = \{r_1, r_2, \dots, r_n\}$, where r_i denotes the position of the i -th atom, and the noisy version of the atom positions is denoted by: $\hat{\mathbf{R}} = \{r_1 + \sigma\epsilon_1, r_2 + \sigma\epsilon_2, \dots, r_n + \sigma\epsilon_n\}$, where σ is the scaling factor and $\epsilon \in \mathcal{N}(\mathbf{0}, \mathbf{I})$. The denoising loss is calculated by the cosine similarity between the predicted and ground-truth noises as:

$$L_{3D} = \frac{1}{B} \sum_{i=1}^B \sum_{j=1}^N [1 - \cos(\epsilon_j^i, \hat{\epsilon}_j^i)], \quad (17)$$

where B denotes the number of graphs in a mini-batch, and $\hat{\epsilon}$ is a prediction output of the model, following the work (Shi et al. 2022; Luo et al. 2023).

Cross-View SSL To better ensure that the shared information retains view-specific information from both 2D and 3D molecular views, we introduce a cross-view SSL task to align the representations across views. Specifically, given 2D representations Z_{2D}^{CIB} , our goal is to infer geometric distance between atoms, without relying on 3D coordinates. The spatial reconstruction loss can be defined as:

$$L_{2D \rightarrow 3D} = \frac{1}{N} \sum_{v_i, v_j} \left\| f\left(\bar{\mathbf{H}}_{2D}^i - \bar{\mathbf{H}}_{2D}^j\right) - D_{ij} \right\|, \quad (18)$$

where $f(\cdot)$ denotes a MLP function and D denotes the distance matrix between atoms v_i and v_j .

Analogously, given the 3D representation \bar{H}_{3D} , we aim to infer the 2D bonding connectivity. Thus, we compute a 2D connectivity loss from the 3D representation, as:

$$L_{3D \rightarrow 2D} = \frac{1}{|V|^2} \|A - Q\|_F^2, \quad (19)$$

where Q is the cosine pairwise similarity matrix of any node pairs in \bar{H}_{3D} . The total loss for the pre-training is as:

$$L = L_{MI} + \beta (L_{2D} + L_{3D} + L_{2D \rightarrow 3D} + L_{3D \rightarrow 2D}), \quad (20)$$

where β controls the trade-off between the compression and reconstruction terms.

Evaluation

Experimental Settings

Datasets We conducted experiments across four different chemical domains: Physiology (BBBP, Tox21, ToxCast, SIDER, ClinTox, and MUV), Physical Chemistry (ESOL,

FreeSolv, and Lipo), Biophysics (mol-HIV and BACE (Wu et al. 2018)), and Quantum Mechanics QM9 (Hu et al. 2021). For the pre-training dataset, we considered 456k unlabeled molecules from the ChEMBL database (Mayr et al. 2018). For the model explainability, we used three datasets, i.e., Benzene, Alkane Carbonyl, and Fluoride Carbonyl, with the presence of ground truth (Agarwal et al. 2023). We evaluated the expressiveness of MVCIB on graph isomorphism testing datasets (Balcilar et al. 2021). We randomly split the datasets into training/validation/test sets with a ratio of 6:2:2. Dataset statistics are described in Appendix B.

Baselines and Implementation Details We considered three baseline groups. The contrastive learning methods are Infomax (Velickovic et al. 2019), JOAO (You et al. 2021), GraphCL (You et al. 2020), and GraphLoG (Xu et al. 2021). The subgraph-based methods are MICRO-Graph (Subramanian 2021), MGSSL (Zhang et al. 2021), GraphFP (Luong and Singh 2023), GROVE (Rong et al. 2020), The multi-view methods are GraphMVP (Liu et al. 2022), Holi-Mol (Kim et al. 2024), and 3D-InfoMax (Stärk et al. 2022). We deliver an open-source implementation of MVCIB for the experiment reproductions¹. The implementation details are presented in Appendix C.

Performance Analysis

Molecular Property Classification Tasks Tab. 1 shows the performance of MVCIB compared to baselines in terms of ROC-AUC on the MoleculeNet dataset. We observed that: (1) MVCIB consistently outperformed baselines on all datasets with a significant improvement. For example, on the BBBP dataset, MVCIB achieved a 3.04% improvement over the second-best model, further demonstrating its effectiveness. (2) MVCIB performed well on multi-task learning datasets, e.g., Tox21 and SIDER, which consist of multiple classification tasks related to toxicity and drug side effect prediction. This indicates that MVCIB effectively captured representations that generalize well across diverse biochemical properties. Moreover, we also demonstrated that MVCIB achieved a significant performance improvement over baselines on regression tasks (Appendix D.2).

3D Geometric Property Regression Tasks Tab. 2 presents the overall performance of MVCIB on seven 3D geometric properties from the QM9 quantum chemistry dataset. We observed that MVCIB consistently outperformed the baselines, achieving the best results on six out of seven tasks, even surpassing models that incorporate additional 3D information, such as GraphMVP and Holo-Mol. For instance, MVCIB achieved a 30.5% improvement in R^2 for predicting electronic spatial extent, effectively capturing electron density within the 3D molecular structure. Notably, MVCIB showed strong performance in predicting isotropic polarizability α , HUMO, and LUMO predictions, showing its ability to learn geometry-aware representations that are essential for predicting quantum mechanical properties.

¹<https://github.com/NSLab-CUK/MVCIB>

Table 1: A performance comparison on classification tasks (ROC-AUC). The top two are highlighted by **first** and **second**.

Methods	BBBP	Tox21	ToxCast	SIDER	ClinTox	MUV	HIV	BACE
Infomax	68.39±0.64	72.66±0.16	62.76±0.54	59.02±0.56	58.62±0.83	72.14±1.25	73.55±0.47	77.80±0.46
JOAO	71.63±1.11	73.67±1.06	63.30±0.27	63.55±0.81	77.02±1.64	69.81±0.26	77.55±1.94	74.94±1.35
GraphCL	68.39±0.64	73.26±0.59	62.76±0.54	61.83±0.60	61.62±1.25	72.14±1.25	73.55±0.47	77.80±0.46
GraphLoG	66.75±0.32	71.64±0.49	61.53±0.35	59.09±0.53	53.76±0.95	72.52±2.02	73.76±0.29	76.60±1.04
GraphFP	72.05±1.17	77.35±1.40	69.15±1.92	65.93±3.09	76.80±1.83	71.82±1.33	75.71±1.39	80.28±3.06
MICRO-Graph	67.21±1.85	71.79±1.70	60.80±1.15	60.34±0.96	77.56±1.56	70.46±1.62	76.73±1.07	63.57±1.55
MGSSL	79.52±1.98	74.82±1.60	63.86±1.57	57.46±1.45	75.84±1.82	73.44±3.47	77.45±2.94	82.03±3.79
GROVE	87.15±0.06	68.59±0.24	64.45±0.14	57.53±0.23	72.53±0.14	67.67±0.12	75.04±0.13	81.13±0.14
S-CGIB	88.75±0.49	80.94±0.17	70.95±0.27	64.03±1.04	78.58±2.01	77.71±1.19	78.33±1.34	86.46±0.81
GraphMVP	68.78±0.24	74.39±0.37	62.65±0.73	61.32±1.41	73.87±1.22	72.83±0.34	76.58±0.64	76.71±0.92
GraphMVP-G	70.76±0.58	74.71±0.29	61.53±0.78	59.59±1.28	74.69±1.82	72.40±0.19	76.34±0.48	77.03±0.81
GraphMVP-C	70.63±0.78	74.46±0.39	62.59±0.49	63.15±1.19	75.68±2.47	74.71±1.27	75.14±1.06	80.99±0.46
Holi-Mol	70.37±0.35	75.11±0.32	61.19±0.38	61.37±0.64	77.81±0.67	75.96±0.56	76.73±0.29	78.82±0.94
3D-InfoMax	68.39±1.35	73.02±1.09	60.73±0.58	56.06±1.33	60.74±1.43	75.31±1.62	74.25±0.95	78.21±1.77
MVCIB (Ours)	90.76±0.45	81.03±0.47	72.28±0.31	67.34±0.31	81.93±1.06	77.92±0.35	79.75±0.51	87.39±0.21

Table 2: A performance comparison on 3D geometric property regression tasks in QM9 dataset in terms of MAE.

Methods	μ	α	HOMO	LUMO	ϵ_{gap}	R^2	zpve
Infomax	21.6427±0.2713	5.8245±0.0497	4.6103±0.0257	22.5401±0.1792	14.4615±0.1526	99.6702±4.8413	28.8924±0.2435
JOAO	13.3878±0.1478	19.2648±0.1783	10.7519±0.1024	18.9824±1.1556	21.2218±1.0699	101.0046±5.8518	25.2529±0.9581
GraphCL	4.4489±0.0822	15.5298±1.0676	7.7433±0.9018	18.8141±0.1287	6.4682±0.0275	127.5179±6.4723	10.8973±0.0285
GraphLoG	5.7881±0.0614	17.2818±0.1397	9.3541±0.6121	15.8762±0.6982	10.5164±0.9695	97.8614±4.3656	12.8907±0.9833
GraphFP	0.5838±0.0174	1.2528±0.0725	0.0074±0.0008	0.0071±0.0003	0.0087±0.0005	53.2751±2.9725	0.0043±0.0001
MICRO-Graph	0.5241±0.0073	1.2649±0.0114	0.0048±0.0009	0.0085±0.0004	0.0079±0.0003	44.1453±2.9864	0.0034±0.0005
MGSSL	0.5746±0.0059	1.0613±0.0128	0.0046±0.0002	0.0047±0.0003	0.0066±0.0008	38.8678±1.7486	0.0083±0.0006
GROVE	0.6113±0.0037	1.0296±0.0124	0.0059±0.0007	0.0051±0.0004	0.0082±0.0008	41.9575±2.0181	0.0071±0.0002
S-CGIB	0.5402±0.0065	3.0022±0.0081	0.0086±0.0006	0.0087±0.0009	0.0115±0.0007	35.7794±0.1638	0.0035±0.0006
GraphMVP	0.5374±0.0093	3.0750±0.0057	0.0062±0.0002	0.0091±0.0007	0.0102±0.0039	85.8648±0.4281	0.0029±0.0005
GraphMVP-G	0.5672±0.0086	2.7505±0.1224	0.0063±0.0001	0.0074±0.0008	0.0105±0.0019	90.1874±4.9913	0.0052±0.0002
GraphMVP-C	0.5578±0.0082	2.8668±0.1915	0.0061±0.0004	0.0075±0.0006	0.0103±0.0017	78.5071±3.2950	0.0034±0.0005
Holi-Mol	0.6441±0.0086	4.4998±0.2511	0.0095±0.0001	0.0103±0.0009	0.0151±0.0076	71.7118±4.8325	0.0028±0.0005
3D-InfoMax	0.6447±0.0051	5.9405±0.7233	0.0117±0.0042	0.0073±0.0009	0.0142±0.0099	77.1154±3.9725	0.0077±0.0005
MVCIB (Ours)	0.5379±0.0063	0.5196±2.7362	0.0042±0.0001	0.0044±0.0000	0.0048±0.0001	24.8314±1.3826	0.0019±0.0000

Representation Quality Analysis

Interpretability Analysis There has been concern regarding the explainability of GNNs, which are black-box. Thus, we conducted experiments to evaluate the quality of MVCIB’s explanations by comparing them with ground-truth structural annotations (Agarwal et al. 2023). We selected the top 50% of nodes with the highest cross-attention weights as the explanations. We used *Fidelity* metrics to evaluate how well the generated explanations align with MVCIB’s predictions, as shown in Tab. 3. We observed that MVCIB consistently outperformed baselines, showing superior interpretability in detecting ground-truth substructures that determine the molecular properties. In addition, qualitative analysis showed that substructures recognized by MVCIB are consistent with the knowledge from chemistry experts, such as the detection of alkane groups (Appendix D.3).

Distinguishability and Alignment Analysis We conducted distinguishability and alignment analyses using Jensen-Shannon Divergence (JSD) on three datasets with functional group labels, as shown in Tab. 4. In the distinguishability experiments (*2D Dist.* and *3D Dist.*), the goal is to assess whether molecular structures with different labels

are distinguishable within each view, where a higher JSD indicates better discrimination. In contrast, the alignment experiment (*2D–3D Align.*) evaluates whether molecular structures with the same label are aligned across views, where a lower JSD shows better alignment. MVCIB achieved the highest JSD scores in the distinguishability tasks and the lowest JSD in the alignment task, showing its ability to discriminate between different molecular structures and consistently align representations across views. In addition, we conducted cross-view reconstruction tasks to evaluate whether the shared information retains features from both molecular views (Appendix D.4). The results showed that the shared representations preserved sufficient view-specific information to reconstruct each view, validating our assumption that all views originate from the same molecule.

Expressiveness Analysis We evaluated the expressive power of MVCIB on isomorphism testing for 1d-WL and 3d-WL datasets. A theoretical analysis of expressiveness is provided in Appendix A.2. Tab. 13 shows the performance on Graph8c and five Strongly Regular Graphs (SRGs): SR1 (16622), SR2 (251256), SR3 (261034), SR4 (281264), and SR5 (291467). We observed that MVCIB successfully distinguished both 1d- and 3d-WL isomorphism datasets,

Table 3: An interpretability comparison on functional group detection tasks in terms of *Fidelity*-/*+*.

Methods	BENZENE		Alkane Carbonyl		Fluoride Carbonyl	
	<i>Fidelity</i> - ↓	<i>Fidelity</i> + ↑	<i>Fidelity</i> - ↓	<i>Fidelity</i> + ↑	<i>Fidelity</i> - ↓	<i>Fidelity</i> + ↑
Infomax	0.363±0.041	0.410±0.082	0.353±0.021	0.376±0.054	0.331±0.032	0.453±0.012
JOAO	0.047±0.005	0.481±0.007	0.263±0.005	0.568±0.008	0.183±0.007	0.295±0.004
GraphCL	0.120±0.005	0.469±0.008	0.430±0.027	0.578±0.016	0.284±0.002	0.570±0.001
GraphLoG	0.137±0.001	0.459±0.007	0.355±0.002	0.695±0.007	0.358±0.004	0.475±0.006
GraphFP	0.093±0.006	0.494±0.012	0.276±0.022	0.529±0.005	0.263±0.026	0.595±0.034
MICRO-Graph	0.140±0.012	0.483±0.003	0.155±0.037	0.524±0.015	0.281±0.007	0.595±0.002
GROVE	0.064±0.029	0.489±0.010	0.183±0.041	0.518±0.007	0.321±0.067	0.628±0.038
S-CGIB	0.049±0.001	0.720±0.003	0.134±0.001	0.727±0.003	0.133±0.002	0.672±0.004
GraphMVP	0.105±0.014	0.374±0.061	0.157±0.003	0.467±0.013	0.430±0.032	0.484±0.037
GraphMVP-G	0.179±0.003	0.369±0.052	0.195±0.004	0.472±0.006	0.115±0.018	0.497±0.028
GraphMVP-C	0.148±0.005	0.485±0.011	0.307±0.009	0.479±0.012	0.255±0.052	0.479±0.033
Holi-Mol	0.058±0.001	0.477±0.016	0.251±0.006	0.472±0.025	0.194±0.011	0.417±0.024
3D-InfoMax	0.037±0.005	0.492±0.012	0.346±0.023	0.466±0.004	0.148±0.046	0.513±0.041
MVCIB (Ours)	0.011±0.003	0.709±0.005	0.118±0.005	0.752±0.003	0.105±0.003	0.708±0.002

Table 4: A Distinguishability (Dist.) and Alignment (Alig.) comparison in terms of Jensen-Shannon Divergence (JSD).

Methods	BENZENE			Alkane Carbonyl			Fluoride Carbonyl		
	2D Dist.↑	3D Dist.↑	2D-3D Alig.↓	2D Dist.↑	3D Dist.↑	2D-3D Alig.↓	2D Dist.↑	3D Dist.↑	2D-3D Alig.↓
GraphMVP	0.113±0.002	0.048±0.000	0.007±0.001	0.093±0.001	0.065±0.001	0.025±0.001	0.166±0.007	0.058±0.001	0.016±0.002
GraphMVP-G	0.094±0.001	0.069±0.001	0.002±0.000	0.104±0.001	0.052±0.001	0.023±0.002	0.192±0.006	0.074±0.001	0.013±0.001
GraphMVP-C	0.124±0.003	0.055±0.001	0.009±0.001	0.094±0.001	0.064±0.002	0.016±0.002	0.183±0.006	0.091±0.002	0.011±0.001
Holi-Mol	0.131±0.003	0.065±0.002	0.012±0.001	0.112±0.002	0.077±0.002	0.021±0.001	0.198±0.003	0.057±0.002	0.014±0.001
3D-InfoMax	0.158±0.007	0.079±0.002	0.016±0.001	0.126±0.002	0.081±0.002	0.032±0.001	0.184±0.003	0.089±0.001	0.008±0.000
MVCIB (Ours)	0.185±0.006	0.094±0.001	0.001±0.000	0.156±0.002	0.108±0.001	0.011±0.002	0.267±0.001	0.116±0.005	0.002±0.000

Table 5: An expressiveness comparison in detecting non-isomorphic graph pairs in 1d- and 3d-WL datasets. An ideal model should distinguish all pairs of non-isomorphic graphs.

Types	1d-WL		3d-WL			
	GRAPH8C	SR1	SR2	SR3	SR4	SR5
Datasets # Graph pairs	61.8M	1	105	45	6	820
GIN	559	1	105	45	6	820
GraphCL	9069	1	105	45	6	532
GraphLoG	7179	1	105	45	6	820
MICRO-Graph	21598	1	105	45	6	820
MGSSL	44102	1	105	45	6	820
S-CGIB	1306	1	105	45	6	820
GraphMVP	1.4M	1	105	45	6	820
Holi-Mol	1.2M	1	105	45	6	820
3D-InfoMax	1.1M	1	105	45	6	820
MVCIB (Ours)	0	0	0	0	0	0

demonstrating its 3d-WL expressive power. This implies that MVCIB effectively captured high-order substructures, which are critical for distinguishing different molecular structures. In addition, MVCIB was capable of distinguishing isomers, which share similar 2D connectivity yet differ in 3D geometry and molecular properties (Appendix D.6).

Model Analysis

Ablation Analysis We evaluated the contributions of the subgraph alignment and MVCIB modules to the overall performance of MVCIB, as shown in Tab. 10. The full re-

Table 6: An ablation analysis on Subgraph Alignment (S.A.) and MVCIB modules.

Methods	ROC-AUC↑			MAE↓		
	BBBP	BACE	Tox21	HOMO	LUMO	ϵ_{gap}
w/o S.A.	89.28	86.95	79.41	0.0067	0.0075	0.0092
w/o MVCIB	89.72	85.09	78.92	0.0061	0.0083	0.0095
MVCIB (Ours)	90.76	87.39	81.03	0.0042	0.0044	0.0048

sults are given in Tab. A4 in the Appendix. This experiment showed that both modules jointly improved model performance, emphasizing their important roles in learning representations for effectively transferring knowledge to downstream tasks. Notably, the MVCIB module showed a significant contribution, indicating its strong ability to capture shared information across molecular views. We also observed that the 2D and 3D structural information are complementary, contributing jointly to the overall performance (Appendix D.5).

Efficiency Analysis We demonstrated that MVCIB with pre-training converges remarkably faster than training from scratch, implying that it learned transferable and well-initialized representations (Appendix D.1).

Sensitivity Analysis In the sensitivity analysis of subgraph size and interatomic distance, MVCIB achieved the optimal performance when the subgraph size is set to 3 and the interatomic distance threshold is 1.5 Å (Appendix D.7).

Regarding the impact of GNN depth, we observed the best performance of MVCIB at $k = 4$ layers (Appendix D.8).

Conclusion

We propose MVCIB, a GNN pre-training method, to improve multi-view learning of molecules by using the MVCIB principle and subgraph-level alignment. Instead of maximizing the agreement between graph-level representations under contrastive objectives, MVCIB explicitly maximizes the shared information across views and minimizes the view-specific information. Moreover, MVCIB could encode important substructures into representations by sampling and aligning them across views, enhancing the learning of chemical substructures during pre-training. By doing so, MVCIB not only achieved superior predictive performance and interpretability but also achieved 3d-WL expressiveness power to distinguish different molecular structures.

References

- Agarwal, C.; Queen, O.; Lakkaraju, H.; and Zitnik, M. 2023. Evaluating explainability for graph neural networks. *Scientific Data*, 10(1): 144.
- Balcilar, M.; Héroux, P.; Gaüzère, B.; Vasseur, P.; Adam, S.; and Honeine, P. 2021. Breaking the Limits of Message Passing Graph Neural Networks. In *Proceedings of the 38th International Conference on Machine Learning (ICML 2021)*, volume 139, 599–608. Virtual Event: PMLR.
- Clayden, J.; Greeves, N.; and Warren, S. 2012. *Organic chemistry*. Oxford university press.
- Degen, J.; Wegscheid-Gerlach, C.; Zaliani, A.; and Rarey, M. 2008. On the art of compiling and using 'drug-like' chemical fragment spaces. *ChemMedChem*, 3(10): 1503.
- Federici, M.; Dutta, A.; Forré, P.; Kushman, N.; and Akata, Z. 2020. Learning Robust Representations via Multi-View Information Bottleneck. In *Proceedings of the 8th International Conference on Learning Representations (ICLR 2020)*. Addis Ababa, Ethiopia.
- Fey, M.; and Lenssen, J. E. 2019. Fast Graph Representation Learning with PyTorch Geometric. In *Proceedings of the ICLR Workshop on Representation Learning on Graphs and Manifolds (ICLRW 2019)*.
- Godwin, J.; Schaarschmidt, M.; Gaunt, A. L.; Sanchez-Gonzalez, A.; Rubanova, Y.; Velickovic, P.; Kirkpatrick, J.; and Battaglia, P. W. 2022. Simple GNN Regularisation for 3D Molecular Property Prediction and Beyond. In *Proceedings of the 10th International Conference on Learning Representations (ICLR 2022)*. Virtual Event.
- Hjelm, R. D.; Fedorov, A.; Lavoie-Marchildon, S.; Grewal, K.; Bachman, P.; Trischler, A.; and Bengio, Y. 2019. Learning deep representations by mutual information estimation and maximization. In *Proceedings of the 7th International Conference on Learning Representations (ICLR 2019)*. New Orleans, LA, USA: OpenReview.net.
- Hoang, V. T.; and Lee, O.-J. 2025. Pre-Training Graph Neural Networks on Molecules by Using Subgraph-Conditioned Graph Information Bottleneck. In *Proceedings of the 39th AAAI Conference on Artificial Intelligence (AAAI 2025)*, volume 39, 17204–17213.
- Hu, W.; Fey, M.; Ren, H.; Nakata, M.; Dong, Y.; and Leskovec, J. 2021. OGB-LSC: A Large-Scale Challenge for Machine Learning on Graphs. In *Proceedings of the 1st Neural Information Processing Systems Track on Datasets and Benchmarks (NeurIPS 2021)*. Virtual Event.
- Huang, Z.; Fan, Z.; Shen, S.; Wu, M.; and Deng, L. 2024. MolMVC: Enhancing molecular representations for drug-related tasks through multi-view contrastive learning. *Bioinformatics*, 40: 190–197.
- Inae, E.; Liu, G.; and Jiang, M. 2023. Motif-aware Attribute Masking for Molecular Graph Pre-training. *arXiv preprint*, arXiv:2309.04589.
- Kim, S.; Nam, J.; Kim, J.; Lee, H.; Ahn, S.; and Shin, J. 2024. Holistic Molecular Representation Learning via Multi-view Fragmentation. *Transactions on Machine Learning Research*, 2024.
- Liu, S.; Wang, H.; Liu, W.; Lasenby, J.; Guo, H.; and Tang, J. 2022. Pre-training Molecular Graph Representation with 3D Geometry. In *Proceedings of the 10th International Conference on Learning Representations (ICLR 2022)*. Virtual Event: OpenReview.net.
- Liu, Z.; Shi, Y.; Zhang, A.; Zhang, E.; Kawaguchi, K.; Wang, X.; and Chua, T. 2023. Rethinking Tokenizer and Decoder in Masked Graph Modeling for Molecules. In *Proceedings of the 36th Advances in Neural Information Processing Systems (NeurIPS 2023)*. New Orleans, LA, USA.
- Luo, S.; Chen, T.; Xu, Y.; Zheng, S.; Liu, T.; Wang, L.; and He, D. 2023. One Transformer Can Understand Both 2D & 3D Molecular Data. In *Proceedings of the 11th International Conference on Learning Representations (ICLR 2023)*. Kigali, Rwanda.
- Luong, K.; and Singh, A. K. 2023. Fragment-based Pretraining and Finetuning on Molecular Graphs. In *Proceedings of the 36th Advances in Neural Information Processing Systems (NeurIPS 2023)*. New Orleans, LA, USA.
- Maron, H.; Ben-Hamu, H.; Serviansky, H.; and Lipman, Y. 2019. Provably Powerful Graph Networks. In *Proceedings of the 32nd on Neural Information Processing Systems (NeurIPS 2019)*, 2153–2164. Vancouver, BC, Canada.
- Mayr, A.; Klambauer, G.; Unterthiner, T.; Steijaert, M.; Wegner, J. K.; Ceulemans, H.; Clevert, D.-A.; and Hochreiter, S. 2018. Large-scale comparison of machine learning methods for drug target prediction on ChEMBL. *Chemical science*, 9(24): 5441–5451.
- Qiu, J.; Chen, Q.; Dong, Y.; Zhang, J.; Yang, H.; Ding, M.; Wang, K.; and Tang, J. 2020. GCC: Graph Contrastive Coding for Graph Neural Network Pre-Training. In *Proceedings of the Conference on Knowledge Discovery and Data Mining (KDD 2020)*, 1150–1160. Virtual Event: ACM.
- Rong, Y.; Bian, Y.; Xu, T.; Xie, W.; Wei, Y.; Huang, W.; and Huang, J. 2020. Self-Supervised Graph Transformer on Large-Scale Molecular Data. In *Proceedings of the 34th Annual Conference on Neural Information Processing Systems (NeurIPS 2020)*. Virtual Event.

- Satorras, V. G.; Hoogeboom, E.; and Welling, M. 2021. E(n) Equivariant Graph Neural Networks. In *Proceedings of the 38th International Conference on Machine Learning (ICML 2021)*, volume 139, 9323–9332. Virtual Event: PMLR.
- Shi, Y.; Zheng, S.; Ke, G.; Shen, Y.; You, J.; He, J.; Luo, S.; Liu, C.; He, D.; and Liu, T. 2022. Benchmarking Graphormer on Large-Scale Molecular Modeling Datasets. *arXiv preprint*, arXiv:2203.04810.
- Stärk, H.; Beaini, D.; Corso, G.; Tossou, P.; Dallago, C.; Günnemann, S.; and Lió, P. 2022. 3D Infomax improves GNNs for Molecular Property Prediction. In *Proceedings of the 10th International Conference on Machine Learning (ICML 2022)*, volume 162 of *PMLR*, 20479–20502. Baltimore, Maryland, USA: PMLR.
- Sterling, T.; and Irwin, J. J. 2015. ZINC 15–ligand discovery for everyone. *Journal of chemical information and modeling*, 55(11): 2324–2337.
- Subramonian, A. 2021. MOTIF-Driven Contrastive Learning of Graph Representations. In *Proceedings of the 35th Conference on Artificial Intelligence (AAAI 2021)*, 15980–15981. Virtual Event: AAAI Press.
- Tishby, N.; Pereira, F. C. N.; and Bialek, W. 2000. The information bottleneck method. *arXiv preprint*, arXiv:physics/0004057.
- Tsai, Y. H.; Wu, Y.; Salakhutdinov, R.; and Morency, L. 2021. Self-supervised Learning from a Multi-view Perspective. In *Proceedings of the 9th International Conference on Learning Representations (ICLR 2021)*. Virtual Event: OpenReview.net.
- Velickovic, P.; Fedus, W.; Hamilton, W. L.; Liò, P.; Bengio, Y.; and Hjelm, R. D. 2019. Deep Graph Infomax. In *Proceedings of the 7th International Conference on Learning Representations (ICLR 2019)*. New Orleans, LA, USA: OpenReview.net.
- Wang, M.; Zheng, D.; Ye, Z.; Gan, Q.; Li, M.; Song, X.; Zhou, J.; Ma, C.; Yu, L.; Gai, Y.; Xiao, T.; He, T.; Karypis, G.; Li, J.; and Zhang, Z. 2019. Deep Graph Library: A Graph-Centric, Highly-Performant Package for Graph Neural Networks. *arXiv preprint arXiv:1909.01315*.
- Wu, Z.; Ramsundar, B.; Feinberg, E. N.; Gomes, J.; Geniesse, C.; Pappu, A. S.; Leswing, K.; and Pande, V. 2018. MoleculeNet: a benchmark for molecular machine learning. *Chemical science*, 9(2): 513–530.
- Xia, J.; Zhao, C.; Hu, B.; Gao, Z.; Tan, C.; Liu, Y.; Li, S.; and Li, S. Z. 2023. Mole-BERT: Rethinking Pre-training Graph Neural Networks for Molecules. In *Proceedings of the 11th International Conference on Learning Representations (ICLR 2023)*. Kigali, Rwanda: OpenReview.net.
- Xu, K.; Hu, W.; Leskovec, J.; and Jegelka, S. 2019. How Powerful are Graph Neural Networks? In *Proceedings of the 7th International Conference on Learning Representations (ICLR 2019)*. New Orleans, LA, USA: OpenReview.net.
- Xu, M.; Wang, H.; Ni, B.; Guo, H.; and Tang, J. 2021. Self-supervised Graph-level Representation Learning with Local and Global Structure. In *Proceedings of the 38th International Conference on Machine Learning (ICML 2021)*, volume 139 of *PMLR*, 11548–11558. Virtual Event: PMLR.
- You, Y.; Chen, T.; Shen, Y.; and Wang, Z. 2021. Graph Contrastive Learning Automated. In *Proceedings of the 38th International Conference on Machine Learning (ICML 2021)*, volume 139 of *PMLR*, 12121–12132. Virtual Event: PMLR.
- You, Y.; Chen, T.; Sui, Y.; Chen, T.; Wang, Z.; and Shen, Y. 2020. Graph Contrastive Learning with Augmentations. In *Proceedings of the 33rd Annual Conference on Neural Information Processing Systems (NeurIPS 2020)*. Virtual Event.
- Zaidi, S.; Schaarschmidt, M.; Martens, J.; Kim, H.; Teh, Y. W.; Sanchez-Gonzalez, A.; Battaglia, P. W.; Pascanu, R.; and Godwin, J. 2023. Pre-training via Denoising for Molecular Property Prediction. In *Proceedings of the 11th International Conference on Learning Representations (ICLR 2023)*. Kigali, Rwanda: OpenReview.net.
- Zhang, J.; Zhang, H.; Xia, C.; and Sun, L. 2020. Graph-Bert: Only Attention is Needed for Learning Graph Representations. *arXiv preprint*, arXiv:2001.05140.
- Zhang, Z.; Liu, Q.; Wang, H.; Lu, C.; and Lee, C. 2021. Motif-based Graph Self-Supervised Learning for Molecular Property Prediction. In *Proceedings of the 34th Advances in Neural Information Processing Systems (NeurIPS 2021)*, 15870–15882. Virtual Event.
- Zhu, J.; Xia, Y.; Wu, L.; Xie, S.; Qin, T.; Zhou, W.; Li, H.; and Liu, T. 2022. Unified 2D and 3D Pre-Training of Molecular Representations. In *Proceedings of the 28th ACM SIGKDD Conference on Knowledge Discovery and Data Mining (KDD 2022)*, 2626–2636. Washington, DC, USA: ACM.

Appendix

A. Proofs

A.1. Proof of Equation 15 in the main text

Recall that given Equation 14 from the main text, our objective is to optimize the loss function L_{MI} , as:

$$L_{MI} = [I(G_{2D}; \mathbf{Z}_{2D}^{CIB} | G_{3D}) + I(G_{3D}; \mathbf{Z}_{3D}^{CIB} | G_{2D})] - \alpha [I(\mathbf{Z}_{2D}^{CIB}; G_{3D}) + I(G_{3D}^{CIB}; G_{2D})]. \quad (21)$$

The first term can be minimized as:

$$\begin{aligned} & I(G_{2D}; \mathbf{Z}_{2D}^{CIB} | G_{3D}) \\ &= \mathbb{E}_{G_{2D}, \mathbf{Z}_{2D}^{CIB}, G_{3D}} \left[\log \frac{p(\mathbf{Z}_{2D}^{CIB} | G_{2D}, G_{3D})}{p(\mathbf{Z}_{2D}^{CIB} | G_{3D})} \right] \\ &= \mathbb{E}_{G_{2D}, \mathbf{Z}_{2D}^{CIB}, G_{3D}} \left[\log \frac{p(\mathbf{Z}_{2D}^{CIB} | G_{2D})}{p(\mathbf{Z}_{2D}^{CIB} | G_{3D})} \right] \\ &= \mathbb{E}_{G_{2D}, \mathbf{Z}_{2D}^{CIB}, G_{3D}} \left[\log \frac{p(\mathbf{Z}_{2D}^{CIB} | G_{2D}) p(\mathbf{Z}_{3D}^{CIB} | G_{3D})}{p(\mathbf{Z}_{3D}^{CIB} | G_{3D}) p(\mathbf{Z}_{2D}^{CIB} | G_{3D})} \right] \\ &= D_{KL}(p(\mathbf{Z}_{2D}^{CIB} | G_{2D}) || p(\mathbf{Z}_{3D}^{CIB} | G_{3D})) \\ &\quad - D_{KL}(p(\mathbf{Z}_{3D}^{CIB} | G_{3D}) p(\mathbf{Z}_{2D}^{CIB} | G_{3D})) \\ &\leq D_{KL}(p(\mathbf{Z}_{2D}^{CIB} | G_{2D}) || p(\mathbf{Z}_{3D}^{CIB} | G_{3D})). \end{aligned} \quad (22)$$

Similarly, we can minimize the upper bound of the second term $I(G_{3D}; \mathbf{Z}_{3D}^{CIB} | G_{2D})$, as:

$$I(G_{3D}; \mathbf{Z}_{3D}^{CIB} | G_{2D}) \leq D_{KL}(p(\mathbf{Z}_{3D}^{CIB} | G_{3D}) || p(\mathbf{Z}_{2D}^{CIB} | G_{2D})). \quad (23)$$

For the third term in Equation 21, the mutual information $I(\mathbf{Z}_{2D}^{CIB}; G_{3D})$ can be reformulated as:

$$\begin{aligned} & I(\mathbf{Z}_{2D}^{CIB}; G_{3D}) \\ &= I(\mathbf{Z}_{2D}^{CIB}; \mathbf{Z}_{3D}^{CIB}, G_{3D}) - I(\mathbf{Z}_{2D}^{CIB}; \mathbf{Z}_{3D}^{CIB} | G_{3D}) \\ &= * I(\mathbf{Z}_{2D}^{CIB}; \mathbf{Z}_{3D}^{CIB}, G_{3D}) \\ &= I(\mathbf{Z}_{2D}^{CIB}; \mathbf{Z}_{2D}^{CIB}) + I(\mathbf{Z}_{2D}^{CIB}; \mathbf{Z}_{2D}^{CIB} | G_{3D}) \\ &\geq I(\mathbf{Z}_{2D}^{CIB}; \mathbf{Z}_{3D}^{CIB}), \end{aligned} \quad (24)$$

where * follows by assuming that \mathbf{Z}_{2D}^{CIB} and \mathbf{Z}_{3D}^{CIB} are conditionally independent given G_{3D} .

Similarly, the fourth term in Equation 21, i.e., $I(\mathbf{Z}_{3D}^{CIB}; G_{2D})$, can be bounded as:

$$I(\mathbf{Z}_{3D}^{CIB}; G_{2D}) \geq I(\mathbf{Z}_{3D}^{CIB}; \mathbf{Z}_{2D}^{CIB}). \quad (25)$$

By plugging Equations 22, 23, 24, and 25 into Equation 21, we have:

$$L_{MI} \leq D_{SKL}(p(\mathbf{Z}_{2D}^{CIB} | G_{2D}) || p(\mathbf{Z}_{3D}^{CIB} | G_{3D})) - \alpha I(\mathbf{Z}_{2D}^{CIB}; \mathbf{Z}_{3D}^{CIB}), \quad (26)$$

where $D_{SKL}(\cdot || \cdot)$ denotes the symmetrized KL divergence between two distributions and α controls the trade-off between the two terms.

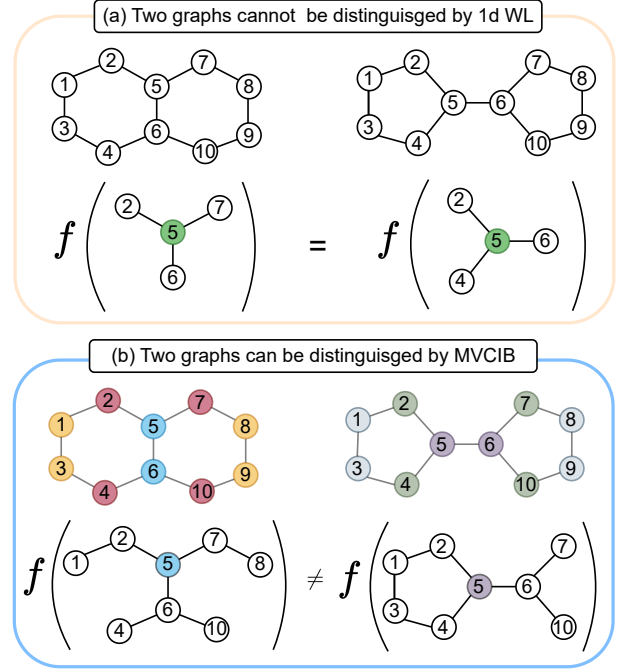


Figure 3: Given a target node v_5 and its surrounding substructures, (a) the 1d Weisfeiler–Lehman (1d-WL) test fails to distinguish the two non-isomorphic substructures rooted at v_5 , even when the observation range is increased. (b) Our proposed model, MVCIB, successfully distinguishes the non-isomorphic substructures. When the observation range is up to 2-hop, the two substructures are different (the edges between nodes at the neighbours of node v_5) and can then be distinguished by our proposed model.

A.2. Proof of Expressiveness Power of MVCIB

Recall that our proposed model, MVCIB, is strictly more powerful than the 1-dimensional and 2-dimensional Weisfeiler–Lehman isomorphism tests (1d- and 2d-WL) in terms of expressiveness.

We first prove that if two graphs are identified as isomorphic by our proposed model, they are also recognized as isomorphic by the 1d-WL test. Then, we present a pair of non-isomorphic graphs that can be distinguished by our proposed model but not by 1d-WL. Together, these results imply that our proposed model is strictly more powerful than 1d-WL. Compared to the 2d-WL test, it can be concluded that 1d-WL and 2d-WL are equivalent in expressiveness for distinguishing graph isomorphism (Maron et al. 2019). In the proof, we use 1-hop ego-network subgraphs for our proposed model.

Assume that given two graphs G and H have the same number of nodes (otherwise easily determined as non-isomorphic) and are two non-isomorphic graphs, but our proposed model determines them as isomorphic. Then for any iteration t , set $\{1d\text{-WL}(G^{(t)}[N_1(v)]) | v \in V_G\}$ is the same as set $\{1d\text{-WL}(H^{(t)}[N_1(v)]) | v \in V_H\}$. Then there exists an ordering of nodes $\{v_1^G, v_2^G, \dots, v_n^G\}$ in G and

$\{v_1^H, v_2^H, \dots, v_n^H\}$ in H , such that for any node order $i = 1, \dots, N$, we have:

$$1\text{d-WL} \left(G^{(t)} [N_1^G(v)] \right) = 1\text{d-WL} \left(H^{(t)} [N_1^H(v)] \right). \quad (27)$$

This implies that they are identical. Thus, it can be deduced that $N_1^G(v)$ and $N_1^H(v)$ are hashed to the same label. Then for any iteration t and any node with order, we have:

$$1\text{d-WL} (N_1^G(v)) = 1\text{d-WL} (N_1^H(v)), \quad (28)$$

where $N_1^G(v)$ and $N_1^H(v)$ denote the set of neighbours of node v . This implies that 1d-WL also fails in distinguishing two non-isomorphic graphs G and H .

In Fig. 3, two graphs are identified as isomorphic by the 1d-WL test, but accurately distinguished as non-isomorphic by MVCIB. Specifically, given a target node v_5 , the 1-dimensional Weisfeiler–Lehman (1d-WL) test fails to distinguish the two substructures rooted at v_5 , even when the observation range is increased, as shown in Fig. 3 (a). In contrast, MVCIB successfully distinguished these non-isomorphic substructures based on distinctions in their surrounding substructures, as shown in Fig. 3 (b). This is because when the observation range is extended to the 2-hop neighborhood, CMVIB successfully distinguished the two substructures. This result demonstrates that incorporating ego-networks enhances the expressive power of the 1d-WL test, enabling it to distinguish graph structures that 1d-WL fails to distinguish.

B. Statistics of Datasets

We provide details on the datasets used in our experiments. For the pre-training dataset, we used 456k unlabeled molecules from the ChEMBL database (Mayr et al. 2018). For the 2D molecular downstream datasets, we utilized benchmark datasets from the MoleculeNet (Wu et al. 2018), including BBBP, Tox21, ToxCast, SIDER, ClinTox, MUV, ESOL, FreeSolv, and Lipo, mol-HIV, and BACE. In addition, for evaluating performance on 3D geometric property regression, we adopted the QM9 dataset (Hu et al. 2021). The detailed statistics for fine-tuning datasets are summarized in Tab. 8. For the datasets used in the interpretability analysis task, we used three datasets, including BENZENE, Alkane Carbonyl, and Fluoride Carbonyl, with their ground-truth explanations (Agarwal et al. 2023), as:

- The BENZENE dataset consists of 12,000 molecules extracted from the ZINC dataset (Sterling and Irwin 2015), where each molecule is labeled with one of two classes based on the presence or absence of a benzene ring.
- The Alkane Carbonyl dataset consists of 1,125 molecules, labeled based on the presence of an unbranched alkane and a carbonyl ($C = O$).
- The Fluoride Carbonyl consists of 8,671 molecules, labeled according to the presence of fluoride (F^-) and a carbonyl ($C = O$).

Table 7: Hyperparameters used in the experiments.

Hyperparameters	Values
Batch size	64
Number of Encoder layers	4
Embedding dimension	300
Number of pre-training epochs	500
Adam: initial learning rate	1×10^{-4}
Adam: weight decay	1×10^{-5}
Readout function	SUM
α	1.0
β	1.0

C. Implementation Details

C.1. Model training The detailed hyperparameter settings are given in Tab. 7. We set the embedding dimension to 300. The hyperparameters α and β are determined with a grid search among $\{0.01, 0.1, 1.0, 10\}$. During the pre-training phase, we train the model for 500 epochs using the Adam optimizer with 1×10^{-4} learning rate and 1×10^{-5} weight decay.

C.2. Baselines We considered three groups of baselines. (1) The contrastive pretraining methods are Infomax (Velickovic et al. 2019), JOAO (You et al. 2021), GraphCL (You et al. 2020), and GraphLoG (Xu et al. 2021). (2) The subgraph-based methods are MICRO-Graph (Subramonian 2021), MGSSL (Zhang et al. 2021), GraphFP (Luong and Singh 2023), GROVE (Rong et al. 2020), and S-CGIB (Hoang and Lee 2025). (3) The multi-view methods are GraphMVP (Liu et al. 2022), Holi-Mol (Kim et al. 2024), 3D-InfoMax (Stärk et al. 2022).

We compare the proposed model against three categories of baselines: (i) contrastive learning methods, (ii) subgraph-based pre-training strategies, and (iii) multi-view pre-training strategies. These baseline methods represent recent SOTA models in self-supervised pre-training for molecular graphs. For fairness, we closely follow the experimental settings reported in the studies.

First, for contrastive learning strategies, we evaluated MVCIB against four methods:

- Infomax (Velickovic et al. 2019) strategy aims to maximize the agreement between the graph-level representations and their sampled subgraphs.
- JOAO (You et al. 2021) strategy generates a set of augmentation schemes, i.e., node dropping, subgraph augmentation, edge perturbation, feature masking, and identical, and tries to automatically find the useful augmentations.
- GraphCL (You et al. 2020) aims at generating multiple views of graphs based on four graph augmentations, i.e., node dropping, edge perturbation, node feature masking, and sampled subgraph, and then maximizes the agreement between these views based on contrastive objectives.
- GraphLoG (Xu et al. 2021) discover the global graph

Table 8: The summary of statistics of datasets used in the experiments.

Category	Dataset	# Tasks	Task Type	# Graphs	Metric	Avg. # nodes
Biophysics	mol-HIV	1	Classification	41,127	ROC-AUC	25.5
	BACE	1	Classification	1,513	ROC-AUC	34.1
Physiology	BBBP	1	Classification	2,039	ROC-AUC	23.9
	Tox21	12	Classification	7,831	ROC-AUC	18.6
	ToxCast	617	Classification	8,575	ROC-AUC	18.7
	SIDER	27	Classification	1,427	ROC-AUC	33.6
	ClinTox	2	Classification	1,478	ROC-AUC	26.1
	MUV	17	Classification	93,087	ROC-AUC	24.2
Physical Chemistry	Lipophilicity	1	Regression	4,200	RMSE	27.0
	ESOL	1	Regression	1,128	RMSE	13.3
	FreeSolv	1	Regression	642	RMSE	8.7
Quantum Mechanics	QM9	12	Regression	133,885	MAE	18.0

structures by using hierarchical prototypes by contrasting graph pairs in a sampled batch.

Second, for subgraph-level pre-training strategies, we considered five methods:

- GraphFP (Luong and Singh 2023) strategy aims to decompose input molecules into a set of subgraphs based on a dictionary (a bag of subgraphs based on subgraph frequent mining), which benefits the model in capturing semantic subgraphs.
- MICRO-Graph (Subramonian 2021) strategy aims to generate a bag of prototypical motifs and automatically learn the important functional group-like motifs.
- MGSSL (Zhang et al. 2021) strategy fragments the input molecules into a bag of functional groups based on an improved algorithm of BRICS by considering ring structures.
- GROVE (Rong et al. 2020) extract 85 functional groups based on discovering frequent subgraphs based on RDKit and utilize a graph transformer architecture.
- S-CGIB (Hoang and Lee 2025) recognizes the core substructures and functional groups under the subgraph-conditioned graph information bottleneck principle.

Third, for multi-view pre-training strategies, we considered three methods:

- GraphMVP (Liu et al. 2022) enhances a 2D molecular graph encoder by integrating rich and discriminative 3D geometric information. There exist two variants of GraphMVP, i.e., GraphMVP-C and GraphMVP-G, which present different contrastive and generative Self-Supervised Learning objectives, respectively.
- HoliMol (Kim et al. 2024) adopts a fragmentation-based approach that decomposes molecules into chemically meaningful substructures, such as functional groups. In addition, HoliMol integrates the 3D geometric view as a complementary view to enrich contrastive learning, capturing both structural and spatial information to enhance molecular representations.

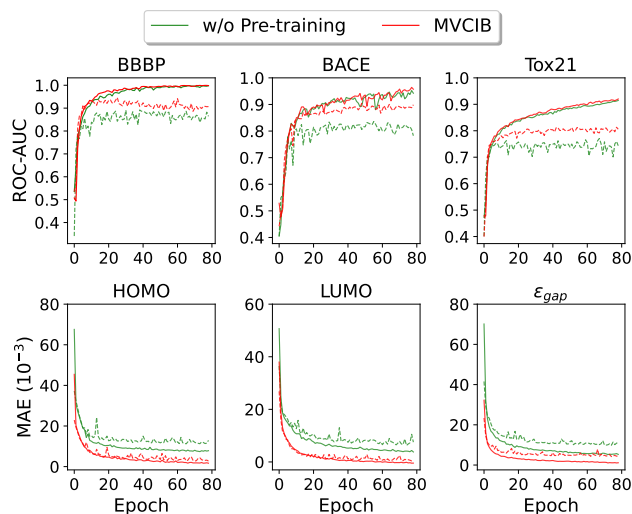


Figure 4: An efficiency analysis for variants of our proposed model: MVCIB with and without pre-training. The solid and dashed lines are training and validation curves, respectively.

- 3D-InfoMax (Stärk et al. 2022) aims to maximize the mutual information between 3D molecular representations and 2D molecular representations. This enables the GNN encoder to implicitly capture and encode 3D geometric information during the pre-training phase.

C.3. Training Resources All experiments were conducted on two servers, each equipped with four NVIDIA RTX A5000 GPUs (24GB RAM/GPU). Our proposed model was implemented and evaluated in Python 3.8.8, using both the PyTorch Geometric framework (Fey and Lenssen 2019) and the Deep Graph Library (DGL) (Wang et al. 2019). All experiments were performed in an Ubuntu 20.04 LTS environment.

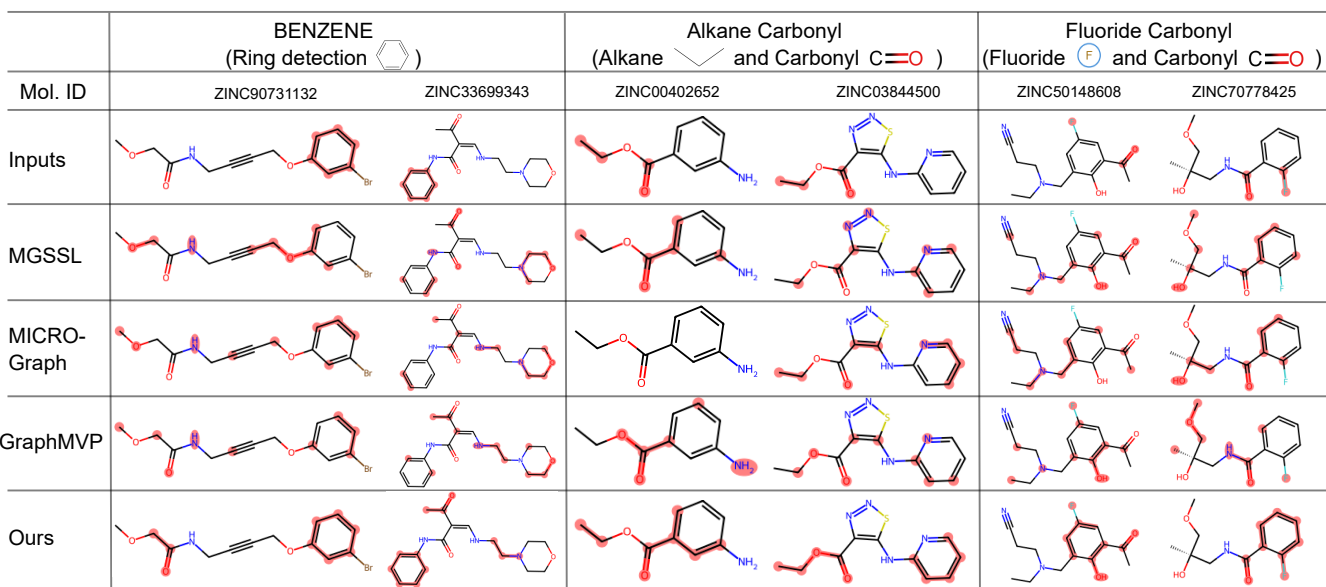


Figure 5: Qualitative analysis on functional group detection tasks.

D. Additional Experiments

D.1. Efficiency Analysis We further evaluated the effects of our proposed model on convergence and generalization capability. As shown in Fig. 4, MVCIB consistently exhibited faster convergence compared to its counterpart trained from scratch, across both molecular property classification (upper) and 3D geometric property regression (lower) datasets. This indicates that the pre-trained model effectively encoded chemical substructures, such as functional groups and local substructures, which serve as strong initialization signals for fine-tuning the models on downstream datasets. Specifically, MVCIB reached optimal performance in significantly fewer training epochs, highlighting its ability to transfer learned information into robust downstream representations. Moreover, the validation curves for MVCIB showed softer and more stable lines, indicating better generalization over unseen molecular data.

D.2. Performance on Regression Tasks We further conducted experiments on three datasets, e.g., FreeSolv, ESOL, and Lipophilicity, in terms of regression tasks, as presented in Tab. 9. We observed that: (1) MVCIB outperformed existing multi-view methods across all three regression datasets, consistently achieving higher predictive accuracy. This indicates that MVCIB more effectively captured chemically meaningful substructures across views, which is essential for predicting molecular regression properties such as solubility and lipophilicity. (2) MVCIB exhibited significant advantages in datasets with a limited amount of labeled data available for training the model. For example, MVCIB achieved an average performance improvement of 9.92% on the ESOL dataset, which comprises only 1,128 labeled molecules. This indicates that MVCIB learned the transferable representations that generalize well and adapt quickly to downstream datasets with limited labeled molecules.

Table 9: A performance comparison on molecular property regression tasks on the MoleculeNet dataset in terms of RMSE. The top two are highlighted by **first** and **second**.

Methods	FreeSolv	ESOL	Lipophilicity
Infomax	3.033±0.026	2.953±0.049	0.970±0.023
JOAO	3.282±0.002	1.978±0.029	1.093±0.097
GraphCL	3.166±0.027	1.390±0.363	1.014±0.018
GraphLoG	2.335±0.052	1.542±0.026	0.932±0.052
GraphFP	2.528±0.016	2.136±0.096	1.371±0.058
MICRO-Graph	1.865±0.061	0.842±0.055	0.851±0.073
MGSSL	2.940±0.051	2.936±0.071	1.106±0.077
GROVE	2.712±0.327	1.237±0.403	0.823±0.027
S-CGIB	1.648±0.074	0.816±0.019	0.762±0.042
GraphMVP	1.129±0.537	0.913±0.006	0.969±0.058
GraphMVP-G	1.068±0.172	0.902±0.027	0.915±0.082
GraphMVP-C	1.082±0.051	0.894±0.025	0.892±0.073
Holi-Mol	2.189±0.077	1.061±0.092	1.182±0.072
3D-InfoMax	2.217±0.126	0.836±0.031	0.915±0.089
MVCIB (Ours)	1.037±0.029	0.735±0.026	0.741±0.085

D.3. Qualitative Analysis Since functional group extraction could act as a bridge between pre-training and downstream molecular property prediction tasks, we are interested in its potential to provide domain-specific interpretability. To qualitatively validate the interpretability of our proposed model, we visualize molecular substructures identified by MVCIB across three datasets: Benzene, Alkane Carbonyl, and Fluoride Carbonyl, as shown in Fig. 5. We observed that MVCIB delivered more accurate and chemically meaningful interpretations compared to baseline methods. It implies that MVCIB could capture and align task-relevant substructures, such as functional groups, during the pre-training phase. By leveraging a subgraph-level alignment strategy guided by cross-attention mechanisms, the sub-

Table 10: An ablation analysis on Subgraph-level Alignment (S.A.) and MVCIB module.

Methods	Classification Tasks (ROC-AUC \uparrow)			3D Geometry Regression Tasks (MAE \downarrow)		
	BBBP	BACE	Tox21	HOMO	LUMO	ϵ_{gap}
w/o S.A.	89.28 \pm 0.51	86.95 \pm 0.58	79.41 \pm 0.39	0.0067 \pm 0.00003	0.0075 \pm 0.00002	0.0092 \pm 0.00003
w/o MVCIB	89.72 \pm 0.31	85.09 \pm 0.94	78.92 \pm 0.66	0.0061 \pm 0.00007	0.0083 \pm 0.00003	0.0095 \pm 0.00008
MVCIB (Ours)	90.76\pm0.45	87.39\pm0.21	81.03\pm0.47	0.0042\pm0.00001	0.0044\pm0.00001	0.0048\pm0.00002

Table 11: A performance comparison on cross-view reconstruction tasks in terms of MSE.

Methods	BBBP	BACE	Tox21	QM9
GraphMVP	0.118 \pm 0.003	0.148 \pm 0.009	0.218 \pm 0.013	0.341 \pm 0.013
GraphMVP-G	0.091 \pm 0.008	0.131 \pm 0.013	0.174 \pm 0.019	0.371 \pm 0.012
GraphMVP-C	0.127 \pm 0.016	0.110 \pm 0.010	0.165 \pm 0.019	0.235 \pm 0.012
Holi-Mol	0.096 \pm 0.005	0.123 \pm 0.011	0.180 \pm 0.102	0.354 \pm 0.009
3D-InfoMax	0.119 \pm 0.017	0.143 \pm 0.010	0.142 \pm 0.012	0.247 \pm 0.021
MVCIB (Ours)	0.031\pm0.003	0.028\pm0.007	0.094\pm0.009	0.121\pm0.005

structures highlighted by MVCIB aligned well with chemical knowledge from experts. Specifically, the model consistently identified important substructures such as benzene rings, alkane chains, and carbonyl groups. These results indicated that beyond improving model transferability, the interpretability offered by MVCIB significantly enhanced trust and practical usability in real-world applications such as drug discovery.

D.4. Cross-View Reconstruction Tasks Motivated by our assumption that different molecular views originate from the same underlying molecule and thus contain shared information across views. Therefore, we conducted ablation studies to validate this hypothesis via cross-view reconstruction tasks on both 2D and 3D molecular datasets, as shown in Table 11. Specifically, for 2D molecular datasets, we employed the Mean Squared Error (MSE) to assess the model’s ability to reconstruct the original adjacency matrix from 3D molecular representations. In contrast, for the 3D dataset, we aimed to reconstruct the interatomic distance based on only the representations from the 2D molecular view. We observed that MVCIB significantly outperformed existing multi-view baselines in reconstructing both 2D topology and 3D geometry structures. Unlike baselines that rely on contrastive learning objectives to maximize mutual information between graph-level representations, MVCIB explicitly focuses on discovering shared information and aligning important substructures across views. This implies the importance of shared information discovery and subgraph-level alignment in learning the correct shared substructures across molecular views. The robust performance in both reconstruction tasks delivered empirical evidence supporting our hypothesis that different molecular views encode complementary yet coherent information derived from the same underlying molecule.

D.5. Ablation Study on Single-View & Multi-View We evaluated the model performance under both multi-view and

single-view settings, as summarized in Tab. 12. That is, we directly used the 2D molecular representations (*2D Only*) or the 3D molecular representations (*3D Only*) as the inputs for property predictions. We observed that jointly leveraging both 2D and 3D molecular representations significantly enhanced predictive performance compared to utilizing either view individually. This implies the complementary effect between learned representations from the two views, where 2D molecular features represent the explicit bond structures and 3D molecular features capture 3D geometric information that is essential for inferring intermolecular interactions. Notably, MVCIB trained exclusively on the 3D view underperformed relative to both the 2D Only and multi-view settings. This performance gap can be attributed to the absence of explicit bond topology in the 3D molecular representations, which can hinder the model’s ability to learn the correct chemical patterns.

D.6. Expressiveness Analysis on Distinguishing Isomers

To evaluate whether our proposed model can capture 3D geometric differences that significantly influence chemical properties, we conducted a study to assess the model’s ability to distinguish isomers, especially on Cis/Trans isomers and Enantiomers, as shown in Tab. 13. Cis/Trans isomers (geometric isomers) arise due to restricted rotation around a double bond or within a ring structure (Clayden, Greeves, and Warren 2012). They are classified based on the relative positions of two similar or high-priority groups: i.e., cis if the groups are on the same side and trans if they are on opposite sides. In contrast, enantiomers are pairs of stereoisomers that are non-superimposable mirror images of one another. These arise when a molecule contains at least one chiral center, resulting in two stereoisomers with identical connectivity but different spatial information.

To the extent of our knowledge, there is no publicly available benchmark molecular dataset designed to evaluate the expressive power of GNNs in distinguishing isomers. To ad-

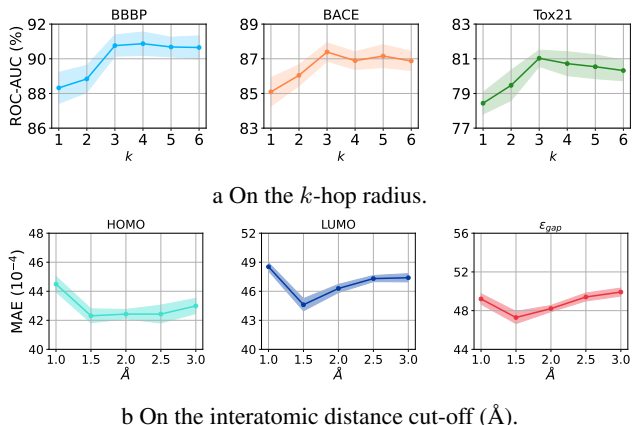
Table 12: An ablation study on single- and multi-view cases.

Methods	Classification Tasks (ROC-AUC \uparrow)			3D Geometry Regression Tasks (MAE \downarrow)		
	BBBP	BACE	Tox21	HOMO	LUMO	ϵ_{gap}
2D Only	88.51 \pm 0.37	86.67 \pm 0.18	79.95 \pm 0.62	0.0072 \pm 0.00004	0.0097 \pm 0.00007	0.0066 \pm 0.00013
3D Only	87.11 \pm 0.43	84.72 \pm 0.32	77.75 \pm 0.87	0.0099 \pm 0.00008	0.0062 \pm 0.00012	0.0052 \pm 0.00003
MVCIB (Ours)	90.76\pm0.45	87.39\pm0.21	81.03\pm0.47	0.0042\pm0.00011	0.0044\pm0.00003	0.0048\pm0.00013

Table 13: An expressiveness comparison in distinguishing isomers. An ideal model should be able to distinguish every isomeric graph pair, as each isomer has different 3D geometry and molecular properties, even though they share the same 2D structures.

Isomer type	Cis/Trans isomers	Enantiomers
# Isomer pairs	500	500
GIN	500	500
JOAO	500	500
GraphCL	500	500
GraphLoG	500	500
MICRO-Graph	500	500
MGSSL	500	500
S-CGIB	500	500
GraphMVP	112	500
Holi-Mol	95	171
3D-InfoMax	106	129
MVCIB (Ours)	0	0

dress this gap, we introduce a new isomer recognition benchmark dataset specifically designed to evaluate GNN performance in distinguishing isomers, such as Cis/Trans isomers and Enantiomers. Specifically, we randomly sampled isomeric molecules from the ZINC15 benchmark database (Sterling and Irwin 2015). For each molecule, we then generate its corresponding isomeric counterpart through expert-guided structural modifications, carefully preserving the smile string while modifying 3D geometric information. The final dataset consists of 500 pairs of Cis/Trans isomers and 500 pairs of Enantiomers. We will release the dataset publicly through our repository to support future research. We observed that: (1) MVCIB consistently distinguished between pairs of isomers, showing the model’s expressiveness in capturing isomeric variations. This implies that MVCIB could capture high-order substructures, e.g., functional groups, and 3D geometric information, which empower MVCIB to recognize 3D geometry differences between isomers. (2) Existing multi-view methods exhibited the ability to differentiate isomers, showing the importance of learning 3D geometric features in molecular learning. However, these models overlooked the identification and alignment of chemical substructures across views, which limits their ability to distinguish isomeric structures. (3) Single-view methods failed to distinguish between isomers due to the absence of explicit 3D geometry information. To sum up, MVCIB

Figure 6: A sensitivity analysis on subgraph sizes: (a) k -hop radius at 2D view and (b) distance cut-off at 3D view.

showed an expressiveness in capturing and aligning high-order chemical substructures across views, enabling it to distinguish isomers.

D.7. Sensitivity Analysis on Subgraph Sizes We further evaluated the performance of our proposed model according to the choice of subgraph size k and interatomic distance cutoff, as shown in Fig. 6. We observed that when k was set to relatively small values, i.e., 3 and 4, our proposed model gained the optimal performance in almost all the datasets. For example, in the BBBP dataset, MVCIB achieved the highest performance when the size $k = 3$, corresponding to a 3-hop subgraph rooted at each node. This implies that the subgraph size could be large enough to capture sufficient and significant subgraphs but not larger, so as to avoid noisy nodes.

Regarding the interatomic distance cutoff, we observed that MVCIB achieved the optimal performance when the cutoff was set to 1.5 \AA . This indicates that a proper cutoff enabled MVCIB to capture the 3D spatial relationships between atoms without noise from irrelevant distant nodes. That is, a small cutoff could overlook the important 3D geometric dependencies, while a too large cutoff value could introduce irrelevant information and degrade the model performance.

D.8. Sensitivity Analysis on the Number of Layers We further validated the performance according to changes in the number of GNN layers, as shown in Fig. 7. We observed that increasing the number of layers, especially to three or

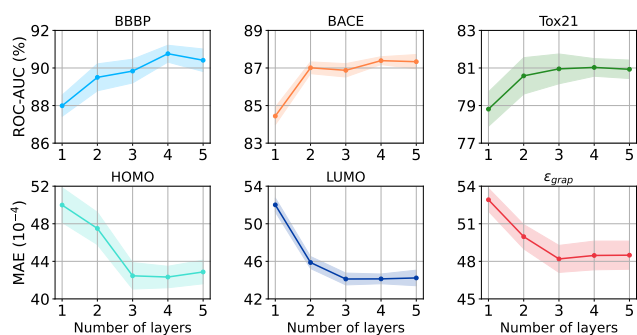


Figure 7: A sensitivity analysis on the number of GNN layers.

four, resulted in significant performance gains compared to other settings. This suggests that a sufficiently deep GNN could enable the model to capture global structural information, which is essential for encoding high-order chemical substructures into the learned representations. However, when the GNN depth continued to increase, the model performance started to degrade. This is because the noisy and irrelevant information could hinder learning correct patterns, which are critical for distinguishing important molecular substructures.